Dynamics of multiphase systems with complex microstructure. II. Particle-stabilized interfaces

Leonard M. C. Sagis*
Food Physics Group, Wageningen University, Bomenweg 2, 6703 HD Wageningen, The Netherlands
and ETH Zurich, Department of Materials, Polymer Physics, Wolfgang-Pauli-Strasse 10, 8093 Zurich, Switzerland
(Received 26 March 2013; published 29 August 2013)

In this paper we use the GENERIC (general equation for nonequilibrium reversible-irreversible coupling) nonequilibrium thermodynamics framework to derive constitutive equations for the surface extra stress tensor of an interface stabilized by a two-dimensional suspension of anisotropic colloidal particles. The dependence of the surface stress tensor on the microstructure of the interface is incorporated through a dependence on a single tensorial structural variable, characterizing the average orientation of the particles. The constitutive equation for the stress tensor is combined with a time-evolution equation describing the changes in the orientation tensor as a result of the applied deformation field. We examine the predictions of the model in in-plane steady shear flow, in-plane oscillatory shear flow, and oscillatory dilatational flow. The model is able to predict the experimentally observed shear thinning behavior in surface shear flow, and also the experimentally observed emergence of even harmonics in the frequency spectrum of the surface stress in oscillatory dilatational flow. Our results show that the highly nonlinear stress-deformation behavior of interfaces with a complex microstructure can be modeled well using simple structural models like the one presented here.

DOI: 10.1103/PhysRevE.88.022150 PACS number(s): 05.70.Ln, 05.70.Np, 47.10.ab, 47.55.N−

I. INTRODUCTION

In a previous paper we presented a general model for the dynamic behavior of multiphase systems with microstructured bulk phases and interfaces, using the GENERIC (general equation for nonequilibrium reversible-irreversible coupling) nonequilibrium thermodynamics framework. Examples of such complex multiphase systems are immiscible polymer blends with compatibilizers adsorbed at the interface, and polymer or particle stabilized emulsions with thickening agents dispersed in the continuous phase. In this paper we present an application of this general model to a specific example: a system with interfaces stabilized by a two-dimensional (2D) suspension of anisotropic colloidal particles.

When nano- or micron-sized particles are used for the stabilization of emulsions and foam, we generally refer to these systems as Pickering emulsions [1] or Pickering foam [2]. Compared to emulsions or foam stabilized by low molecular weight surfactants, particle stabilized systems have a much higher stability against coalescence [3]. The increase in stability is thought to be the result of an increase in the rheological properties of the interfaces (the surface shear and dilatational modulus) [3]. Surface rheological experiments on interfaces stabilized by spherical colloidal particles [4–9], and anisotropic particles [10], confirm the increase in surface rheological properties, compared to interfaces stabilized with low molecular weight surfactants.

At equal surface coverage, interfaces with adsorbed anisotropic colloidal particles tend to have higher values for their surface rheological properties than interfaces with spherical ones [11,12], and for interfaces with anisotropic particles these properties also tend to have a more complex dependence on surface loading than those of interfaces with spherical particles [12]. This more complex dependence of the rheological response on surface concentration is the result of an increase in complexity of the microstructure of the interface, and the response of that microstructure to applied deformations.

With the analysis presented in this paper we show that the complex rheological behavior of this type of system can be modeled well using structural models that link the response of a system to an applied deformation directly to the time evolution of its microstructure. Microstructural modeling has been applied extensively to single phase materials with microstructured bulk phases, such as polymer melts, polymer solutions, colloidal suspensions, or nematic phases [13,14]. In surface rheology this type of modeling has not yet received much attention [15].

Most Pickering stabilized systems tend to have relatively high surface loadings, close to the 2D dense packing limit. For the sake of simplicity we will focus here on interfaces in the dilute particle concentration regime. This means that we cannot compare our predictions quantitatively to experimental data, since the stresses in dilute particle stabilized interfaces tend to be in the range 10^{-9}–10^{-7} Pa m, well below the range of available surface shear and dilatational rheometers. But we can still compare our predictions in a qualitative manner. We will show that the GENERIC model we present here can predict the shear thinning behavior typically observed experimentally for particle stabilized interfaces in steady and oscillatory shear flow. Our model also predicts the emergence of even harmonics in the frequency spectrum in dilatational deformations, a phenomenon recently observed in Langmuir trough experiments on polymer stabilized interfaces [16,17]. We will show that all these phenomena can be linked directly to changes of the orientation of the anisotropic particles as a result of the applied deformation field. Combining structural models like the one we will present here, with advanced experimental techniques such as FT rheology and optical methods for structure evaluation (surface rheo-optics), will enable us to make significant progress in the study of the dynamics of complex interfaces.

*leonard.sagis@wur.nl

II. INTERFACES WITH ANISOTROPIC COLLOIDAL PARTICLES

We will now discuss specific forms of the GENERIC model presented in the previous paper, for a multiphase system with interfaces stabilized by a 2D suspension of anisotropic colloidal particles. We will consider a flat fluid-fluid interface, between two isotropic bulk fluids, which do not contain any microstructural elements. The interface is perturbed by either a steady shear flow, an oscillatory shear flow, or an oscillatory dilatational flow field. We will assume that the particle concentration in the interface is in the dilute regime, and the interactions between the particles are such that the dilute 2D dispersion formed by the particles is stable against aggregation. The surface area not covered by the particles can be either free of surfactant or may have a low molecular weight surfactant adsorbed to it, which does not immobilize the interface or impart any elasticity to it. We will assume that the particles have adsorbed irreversibly, so the total adsorbed mass of particles is constant in time. This particular system was recently described in the context of the classical irreversible thermodynamics formalism [18], and we will compare the expressions derived in that study quantitatively with results derived using our GENERIC model.

The first step in describing this particular example is the selection of the appropriate structural variables. This system is adequately described with a single scalar surface variable, which we choose to be the surface particle density ρ_P^s, and a single surface tensorial variable, representing the orientation of the particles. For the tensorial variable we have several possibilities, all involving the second moment of the distribution of the particle orientation vector $\mathbf{n}^s$, a unit vector representing the direction of the long axis of the particles. Since we have assumed that we are in the dilute particle concentration regime it is reasonable to assume that the particles on average will be oriented parallel to the interface. If we assume that fluctuations in the component of $\mathbf{n}^s$ perpendicular to the interface around an average value of zero are negligible, we may use a tangential surface tensor to describe the microstructure of the interface. One of the possible choices for the tensorial variable is

$$\mathbf{Q}^s = \left\langle \mathbf{n}^s\mathbf{n}^s - \tfrac{1}{2}\mathbf{P} \right\rangle_s, \tag{1}$$

where $\langle\cdots\rangle_s$ denotes a local average over a portion of the interface, and $\mathbf{P}$ is the surface projection tensor (this tensor transforms every tangential surface vector field into itself, and every nontangential surface vector field into its tangential component [19]). The tensor $\mathbf{Q}^s$ is a symmetric traceless tangential surface tensor. At equilibrium the particles are oriented randomly, and the value of the components of this tensor are identical to zero. When the interface is perturbed by a simple shear flow, the particles will start to orient in the direction of the flow field, and the components will attain nonzero values. Alternatively, we can choose the tensorial variable to equal

$$\mathbf{C}^s = 2\langle \mathbf{n}^s\mathbf{n}^s \rangle_s. \tag{2}$$

This tensor is normalized such that at equilibrium $\mathbf{C}^s_{eq} = \mathbf{P}$, and $\mathrm{tr}\mathbf{C}^s = 2$. This tensor gives slightly less complicated expressions for the evolution equations than the tensor in (1), and therefore we proceed with this particular form. The CIT model in Ref. [18] used (1) as a tensorial variable. But we can easily convert results for this tensor to the tensor used here. For a flat interface in a Cartesian surface coordinate system (x,y), the components of these tensors are related by

$$Q^s_{xx} = \tfrac{1}{2}C^s_{xx} - \tfrac{1}{2}, \quad Q^s_{xy} = \tfrac{1}{2}C^s_{xy}. \tag{3}$$

The next step in modeling this system is to choose an expression for the configurational surface Helmholtz free energy in terms of the structural parameters. We will assume that there is no contribution to the free energy from the configurational internal energy $\bar{U}^s_c$, so the contributions to $\bar{F}^s_c$ are purely entropic. For small departures from equilibrium this free energy is often simply expanded in terms of the structural variables. But here we want our equations to be valid also far from equilibrium. We therefore choose [14,20]

$$\bar{F}^s_c = \frac{k_B T^s \rho^s \omega^s_P}{m}\left(\ln \omega^s_P - \frac{1}{2}[\mathrm{tr}(\mathbf{P} - \mathbf{C}^s) + \ln\det \mathbf{C}^s] \right), \tag{4}$$

where k_B is the Boltzmann constant, $\omega^s_{(P)}$ is the surface mass fraction of the particles (equal to $\rho^s_{(P)}/\rho^s$), and m is the mass of a single colloidal particle. This expression gives us the following equation for the surface extra stress tensor [using Eq. (47) from the previous paper]:

$$\boldsymbol{\sigma}^s_{\mathrm{tot}} = (\varepsilon_d - \varepsilon_s)\,[\nabla_s \cdot \mathbf{v}^s]\mathbf{P} + 2\varepsilon_s \mathbf{D}^s + \frac{k_B T^s \rho^s \omega^s_P}{m}(\mathbf{C}^s - \mathbf{P}), \tag{5}$$

where ε_s is the surface shear viscosity of the bare interface, ε_d is the surface dilatational viscosity of the bare interface, ∇_s denotes the surface gradient operator, $\mathbf{v}^s$ is the surface velocity field, and $\mathbf{D}^s$ is the surface rate of deformation tensor [19]. The first two terms in this expression represent the contributions to the surface stress induced by the bare interface. For these contributions we have assumed a linear Boussinesq model [21–23]. The last term in (5) represents the contributions from the microstructure to the total surface stress.

We will assume that the flow field does not induce in-plane spatial gradients in the particle concentration and particle orientation. Hence the diffusive terms in (56) and (60) in the previous paper [24] are identical to zero. Since we have assumed that the structural elements are confined to the interface, and their concentration in the bulk is zero, we may also drop the boldface jump terms in these expressions, since these describe the transfer of particles between the interface and the adjoining bulk phases. In view of these assumptions, (56) from the previous paper is satisfied identically, and (60) reduces to

$$\frac{\partial \mathbf{C}^s}{\partial t} - \mathbf{C}^s \cdot (\nabla_s \mathbf{v}^s)^T - (\nabla_s \mathbf{v}^s)\cdot \mathbf{C}^s - 4H\mathbf{v}^s \cdot \mathbf{C}^s \boldsymbol{\xi} + \frac{k_B \rho^s \omega^s_P}{m}\mathbf{R}^s_2 : (\mathbf{P} - [\mathbf{C}^s]^{-1}) = 0, \tag{6}$$

where H is the curvature of the interface, $\boldsymbol{\xi}$ denotes the unit vector normal to the interface, and $\mathbf{R}_2$ is a fourth order surface tensor describing relaxation effects for the orientation of the particles. To complete the model, we need to specify the tensor

$\mathbf{R}_2^s$. We will assume this tensor is given by

$$\mathbf{R}_2^s = \frac{m}{k_B\rho^s\omega_P^s}\frac{1}{\tau}\big(a_{\alpha\mu}C^s_{\beta\nu} + a_{\alpha\nu}C^s_{\beta\mu} + \beta\big[C^s_{\alpha\mu}C^s_{\beta\nu} + C^s_{\alpha\nu}C^s_{\beta\mu}\big]\big)\mathbf{a}^\alpha\mathbf{a}^\beta\mathbf{a}^\mu\mathbf{a}^\nu, \quad (7)$$

where τ is a characteristic time associated with the relaxation of the orientation tensor, $a_{\alpha\beta}$ denotes the surface metric [19], and the unit vectors $\mathbf{a}^\alpha$ ($\alpha = 1,2$) denote the dual basis for the tangential vector fields [19]. For rigid anisotropic particles the relaxation time τ is inversely proportional to the rotational diffusion coefficient of the particles in the interface. The rotational diffusion coefficient is a function of the characteristic dimensions of the particles, and particle concentration, so τ is completely determined by the same parameters. When the interface is still close to an isotropic state, the linear terms in (6) are sufficient to describe the relaxation processes. The coefficient β characterizes the magnitude of the nonlinear corrections for the linear relaxation behavior, which become important when the system is highly anisotropic [14]. With this particular expression for the tensor $\mathbf{R}_2^s$, Eq. (6) reduces to

$$\frac{\partial\mathbf{C}^s}{\partial t} - \mathbf{C}^s\cdot(\boldsymbol{\nabla}_s\mathbf{v}^s)^T - (\boldsymbol{\nabla}_s\mathbf{v}^s)\cdot\mathbf{C}^s - 4H\mathbf{v}^s\cdot\mathbf{C}^s\boldsymbol{\xi} + \frac{1}{\tau}([1-\beta]\mathbf{C}^s - \mathbf{P} + \beta\mathbf{C}^s\cdot\mathbf{C}^s) = 0. \quad (8)$$

We see that this particular choice for $\mathbf{R}_2^s$ results in a two parameter model for the evolution of the surface orientation tensor, in which τ is determined by the particle dimensions and particle concentration, and β is an adjustable parameter. In the next sections we will examine the predictions of this model in steady in-plane shear flow, oscillatory in-plane shear, and oscillatory dilatational flow.

III. STEADY IN-PLANE SHEAR

We will now consider some specific results for this model, for a flat interface, perturbed by a simple shear flow, with constant shear rate. We will use a Cartesian coordinate system, in which (x,y) denote the surface coordinates, and z is the coordinate in the direction perpendicular to the interface. For a simple in-plane shear flow, with $(\boldsymbol{\nabla}_s\mathbf{v}^s)_{xy} = \dot\gamma$, where $\dot\gamma$ denotes the shear rate (constant in time), and $(\boldsymbol{\nabla}_s\mathbf{v}^s)_{xx} = (\boldsymbol{\nabla}_s\mathbf{v}^s)_{yy} = 0$, the xy component of the surface extra stress tensor will take the form

$$\sigma^s_{\mathrm{tot},xy} = \varepsilon_s\dot\gamma + \left(\frac{k_BT^s\rho^s\omega_P^s}{m}\right)C^s_{xy} \quad (9)$$

and from this we obtain the following expression for the effective surface shear viscosity $\varepsilon_s^{\mathrm{eff}} = \sigma^s_{\mathrm{tot},xy}/\dot\gamma$:

$$\varepsilon_s^{\mathrm{eff}} = \varepsilon_s + \left(\frac{k_BT^s\rho^s\omega_P^s}{m}\right)\frac{C^s_{xy}}{\dot\gamma}. \quad (10)$$

For the xx and xy components of (8) we obtain

$$\frac{\partial C^s_{xx}}{\partial t} = 2\dot\gamma C^s_{xy} - \frac{1}{\tau}\big([1-\beta]C^s_{xx} - 1 + \beta\big[\big(C^s_{xx}\big)^2 + \big(C^s_{xy}\big)^2\big]\big), \quad (11)$$

$$\frac{\partial C^s_{xy}}{\partial t} = \dot\gamma\left(2 - C^s_{xx}\right) - \frac{1}{\tau}[1+\beta]C^s_{xy}. \quad (12)$$

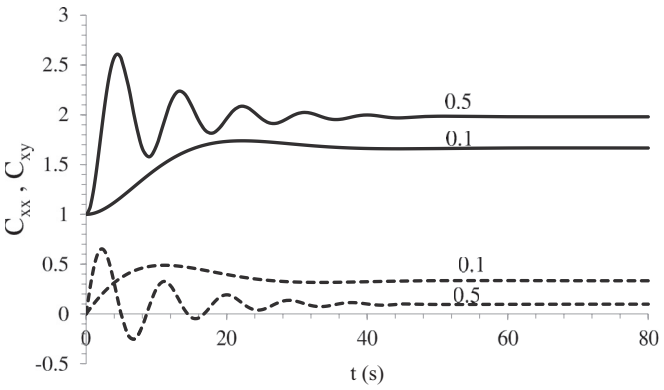

FIG. 1. C^s_{xx} (solid lines) and C^s_{xy} (dashed lines) as a function of time, for a relaxation time τ equal to 10 s, calculated using (13), and (14). The label next to the lines represents the applied shear rate $\dot\gamma$.

For $\beta = 0$ this reduces to a system of linear equations with an analytical solution of the form

$$C^s_{xx} = \frac{1}{1+2\dot\gamma^2\tau^2}[1 + 4\dot\gamma^2\tau^2 - 2\dot\gamma^2\tau^2\cos(\sqrt{2}\dot\gamma t)e^{-t/\tau} - \sqrt{2}\dot\gamma\tau\sin(\sqrt{2}\dot\gamma t)e^{-t/\tau}], \quad (13)$$

$$C^s_{xy} = \frac{\dot\gamma\tau}{1+2\dot\gamma^2\tau^2}[1 - \cos(\sqrt{2}\dot\gamma t)e^{-t/\tau} + \sqrt{2}\dot\gamma\tau\sin(\sqrt{2}\dot\gamma t)e^{-t/\tau}]. \quad (14)$$

In Fig. 1 we plot the time evolution of C^s_{xx} and C^s_{xy} as a function of time, calculated using (13) and (14), for a value of the relaxation time τ equal to 10 s, and two values for the applied shear rate $\dot\gamma$ (0.1 and 0.5 s^{-1}). We see that for $\tau\dot\gamma \leqslant 1$, both components evolve smoothly to their steady state value, whereas for $\tau\dot\gamma \geqslant 1$ significant oscillations can be observed in the evolution of both components. In the latter case we see that although the steady state value for C_{xx} is less than 2, the first oscillations exceed this value significantly, which is nonphysical. So for $\beta = 0$, which corresponds to a linearized version of (11) and (12), the model clearly gives realistic predictions only for $\tau\dot\gamma \leqslant 1$. For $\tau\dot\gamma \geqslant 1$ the full version of (11) and (12) should be used.

The steady state values for (13) and (14), obtained in the limit $t \to \infty$, equal

$$C^s_{xx} = \frac{1+4\dot\gamma^2\tau^2}{1+2\dot\gamma^2\tau^2}, \quad (15)$$

$$C^s_{xy} = \frac{\dot\gamma\tau}{1+2\dot\gamma^2\tau^2}. \quad (16)$$

From this we find

$$\lim_{\dot\gamma\to 0}\frac{C^s_{xy}}{\dot\gamma} = \tau \quad (17)$$

and combining this with (10), we find that the zero surface shear viscosity of the 2D dispersion of anisotropic particles is equal to

$$\varepsilon_0 = \varepsilon_s + \left(\frac{k_BT^s\rho^s\omega_P^s}{m}\right)\tau. \quad (18)$$

So our model predicts a zero surface shear viscosity which depends on concentration and dimensions of the particle

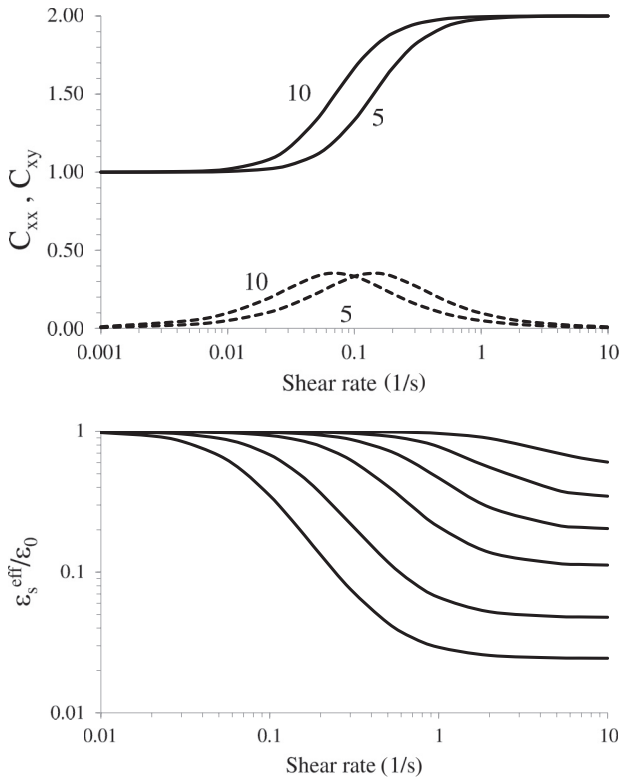

FIG. 2. (a) C^s_{xx} (solid lines) and C^s_{xy} (dashed lines) as a function of shear rate, for a relaxation time τ equal to 5 or 10 s, calculated using (13), and (14); (b) $\varepsilon_s^{\text{eff}}/\varepsilon_0$ as a function of shear rate, for relaxation times equal to (top to bottom) 0.2, 0.5, 1.0, 5.0, and 10 s ($T^s = 290$ K, $\rho^s = 1 \times 10^{-6}$ kg/m^2, $\omega_P^s = 0.01$, $m = 1 \times 10^{-20}$ kg, $\varepsilon_s = 1 \times 10^{-9}$ Pa m s^{-1}).

(through τ). In Fig. 2 we have plotted C^s_{xx}, C^s_{xy}, and $\varepsilon_s^{\text{eff}}/\varepsilon_0$, calculated using (10), (13), and (14), as a function of the applied shear rate $\dot\gamma$, for several values of the relaxation time τ (0.2, 0.5, 1.0, 5.0, and 10 s). We see that the single-parameter version of our model is able to describe the shear thinning behavior typically observed for this type of interface [10–12]. In the region of the plots in Fig. 1(b), where the effective surface shear viscosity is decreasing with an almost linear slope (on a log-log plot), we have analyzed that decrease with a power-law dependence, $\varepsilon_s^{\text{eff}}/\varepsilon_0 \sim \dot\gamma^n$. The parameter n is plotted as a function of τ in Fig. 3. We see that for large values of τ the exponent n takes on nonphysical values (<-1.0). In this regime the model overestimates the shear thinning behavior and we will have to take nonlinear relaxation contributions into account ($\beta \neq 0$).

We have solved the full equations (11) and (12) numerically, using a simple forward Euler scheme, with a time step $\Delta t = 5 \times 10^{-5}$ s, for several values of β (equal to 0, 0.3, 0.5, 1.0, 3.0, 5.0), and a value of τ equal to 10 s. In Fig. 4(a) we have plotted $\varepsilon_s^{\text{eff}}/\varepsilon_0^s$ as a function of shear rate, for these values of β, and we see that for increasing values of this parameter the degree of shear thinning is reduced. The exponent n for these curves is plotted in Fig. 4(b) and we see that this exponent increases from a value of about -1.3 for β equal to 0, to a value of about -0.8 for $\beta = 5$. So the parameter β allows us to extend the range where the model gives physical predictions to much higher values for $\tau\dot\gamma$ (of the order of 100).

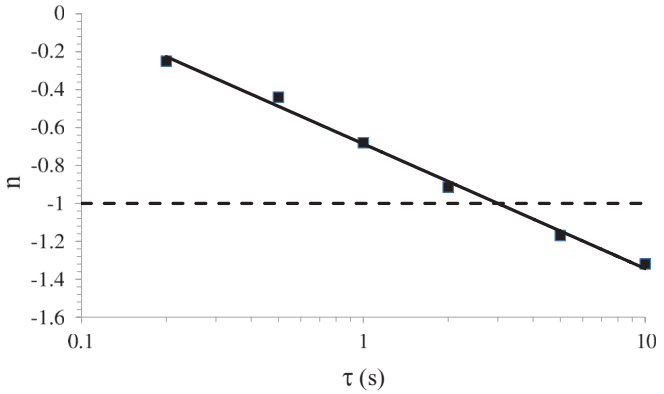

FIG. 3. (Color online) The exponent n as a function of relaxation time τ; n was determined by fitting the results in Fig. 2(b) with the relation $\varepsilon_s^{\text{eff}}/\varepsilon_0 \sim \dot\gamma^n$.

An important feature of our model is that the effective surface shear viscosity remains positive, even for large values of the shear rate (since in the limit $\dot\gamma \to \infty$, $\varepsilon_s^{\text{eff}} \to \varepsilon_s$). This is in contrast to the values obtained for this parameter with the CIT model developed in Ref. [18]. The latter model severely overestimates the shear thinning effect, and may produce nonphysical negative values for the effective surface shear

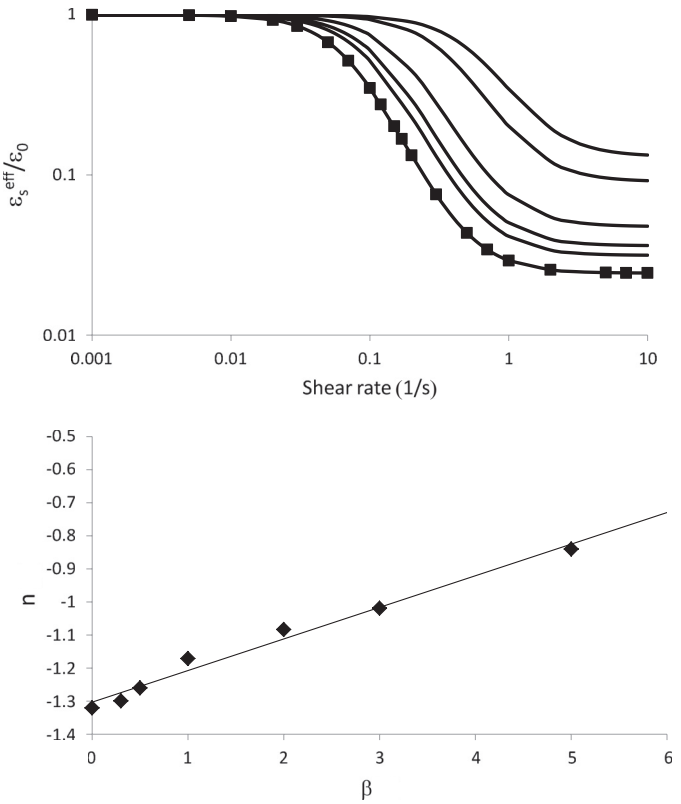

FIG. 4. (a) $\varepsilon_s^{\text{eff}}/\varepsilon_0$ as a function of shear rate, for a relaxation time equal to 10 s, and values for β equal to (bottom to top) 0, 0.3, 0.5, 1.0, 3.0, and 5.0. Squares denote the analytical solution for $\beta = 0$ ($T^s = 290$ K, $\rho^s = 1 \times 10^{-6}$ kg/m^2, $\omega_P^s = 0.01$, $m = 1 \times 10^{-20}$ kg, $\varepsilon_s = 1 \times 10^{-9}$ Pa m s^{-1}). (b) Exponent n as a function of β, where n was determined by fitting the results in Fig. 4(a) with the relation $\varepsilon_s^{\text{eff}}/\varepsilon_0 \sim \dot\gamma^n$.

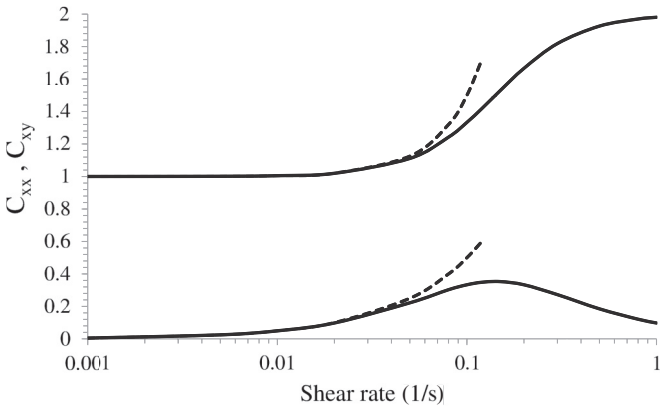

FIG. 5. C^s_{xx} (top two curves) and C^s_{xy} (bottom two curves) as a function of shear rate, for a relaxation time τ equal to 5 s, calculated using (13) and (14) (solid curves) or the CIT model (dashed curves) described in Ref. [18].

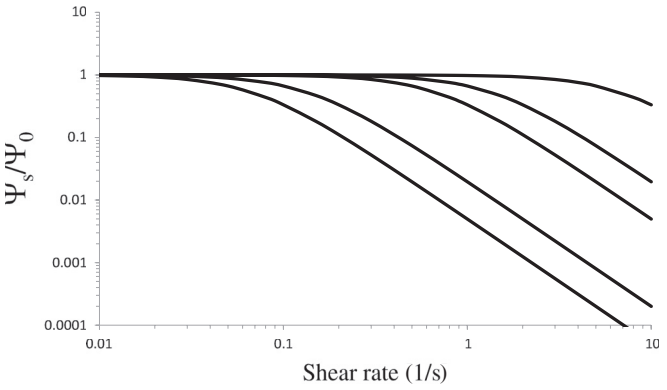

FIG. 6. Steady state value of Ψ_s/Ψ_0, as a function of shear rate, for relaxation times τ equal to (top to bottom) 0.1, 0.5, 1, 5, and 10 s ($T^s = 290$ K, $\rho^s = 1 \times 10^{-6}$ kg/m^2, $\omega^s_P = 0.01$, $m = 1 \times 10^{-20}$ kg, $\varepsilon_s = 1 \times 10^{-9}$ Pa m s^{-1}).

viscosity, when shear rates exceed 0.1 s^{-1}. In Fig. 5 we have plotted C^s_{xx} and C^s_{xy} as a function of the applied shear rate, calculated with our single-parameter model (solid curves), and a linearized version of the CIT model from Ref. [18] (setting the parameters in this model equal to $\tilde{L}^s_1 = 1$, $\tilde{L}^s_2 = 2/3$, $\tilde{L}^s_3 = \tilde{\nu}_3 = 0$, and $D^s_r = 1/2\tau$). We see that up to shear rates of approximately 0.05 s^{-1} both models give good agreement for the time evolution of the orientation tensor. But above a shear rate of 0.1 s^{-1} the CIT model deviates significantly, and gives nonphysical values for both C^s_{xx} and C^s_{xy}.

Another interesting feature of our single-parameter model is that in steady in-plane shear it predicts the existence of nonzero surface normal stresses. These stresses are not to be confused with stresses normal to the interface (in this case the z direction). They are normal to the direction of flow, i.e., the are pointing in the y direction. From (5) we find that the surface normal stress difference equals

$$\sigma^s_{\mathrm{tot},xx} - \sigma^s_{\mathrm{tot},yy} = \left(\frac{2k_B T^s \rho^s \omega^s_P}{m}\right)\left(C^s_{xx} - 1\right) \qquad (19)$$

and this allows us to express the surface normal stress coefficient $\Psi_s = (\sigma^s_{\mathrm{tot},xx} - \sigma^s_{\mathrm{tot},yy})/\dot{\gamma}^2$ as

$$\Psi_s = \left(\frac{2k_B T^s \rho^s \omega^s_P}{m}\right)\frac{C^s_{xx} - 1}{\dot{\gamma}^2}. \qquad (20)$$

From this expression, and (15), we find that the zero shear normal stress coefficient is given by

$$\Psi_0 = \left(\frac{4k_B T^s \rho^s \omega^s_P}{m}\right)\tau^2. \qquad (21)$$

In Fig. 6 we have plotted Ψ_s/Ψ_0, calculated using (15) and (20), as a function of the applied shear rate, for five values of the relaxation time τ (from top to bottom 0.1, 0.5, 1, 5, and 10 s). We see that the surface normal stress coefficient decreases with shear rate as $\Psi_s/\Psi_0 \sim \dot{\gamma}^{-2}$. At the present time the existence of in-plane normal forces has not yet been confirmed experimentally. But by analogy with microstructured bulk phases, we would expect such normal forces to exist. In a surface shear experiment using a bicone geometry [25,26], they would be directed towards the axis of the geometry, and could cause "cone climbing," an effect similar to rod climbing observed in 3D rheology.

IV. OSCILLATORY IN-PLANE SHEAR

We will now explore the predictions of our GENERIC model in oscillatory in-plane shear. We will assume that the applied surface strain is given by $\gamma(t) = \gamma_0 \sin(2\pi\omega t)$, where γ_0 is the strain amplitude, and ω is the frequency of oscillation. The resulting shear rate is given by $(\nabla_s \mathbf{v}^s)_{xy} = \dot{\gamma}(t) = 2\pi\omega\gamma_0 \cos(2\pi\omega t)$. The stress response to such a deformation is given by $\sigma^s_{\mathrm{tot},xy} = \sigma_0 \sin(2\pi\omega t + \delta)$, where σ_0 is the amplitude of the surface shear stress, and δ is a phase shift [15,19,27]. We solved (11) and (12) numerically, again using a forward Euler scheme, and adjusting the time step to a value such that we obtain 1024 data points per cycle. We simulated for a total of 30 cycles, and to eliminate start-up effects from the analysis, the first ten strain cycles are omitted from the analysis. We fixed β to zero, and the frequency was kept fixed at 0.1 Hz. Simulations were performed for two values of τ, 1.0 and 10 s respectively, which corresponds to values for $\omega\tau$ equal to 0.1 and 1.0. The stress response was analyzed using a fast Fourier transform (FFT) to determine the amplitude σ_0, the phase shift δ, and the intensities of the higher harmonics in the frequency spectrum of the stress response. The latter were used to study the nonlinearity of the response (FT rheology [28–30]).

Figure 7(a) shows typical results for the surface shear stress as a function of time, for strain amplitudes γ_0 equal to 0.1, 0.5, 1.0, and 3.0. For the highest amplitudes we see a clearly nonlinear response, induced by the changes in the microstructure of the interface. Figures 7(b) and 7(c) show Lissajous plots for $\omega\tau$ equal to 0.1 and 1.0 respectively. The response is typical for a viscoelastic interface. At low values for the strain amplitude, the interface displays a viscous behavior at low values for $\omega\tau$, and a more elastic behavior for high values of $\omega\tau$. For $\omega\tau = 1.0$ the interface shows a transition from elastic behavior to viscous behavior as the amplitude is increased.

This behavior can also be seen in the strain sweeps presented in Fig. 8. This figure gives the results for the surface storage modulus G'_s and surface loss modulus G''_s as a function of the applied strain, for $\omega\tau$ equal to 0.1 and

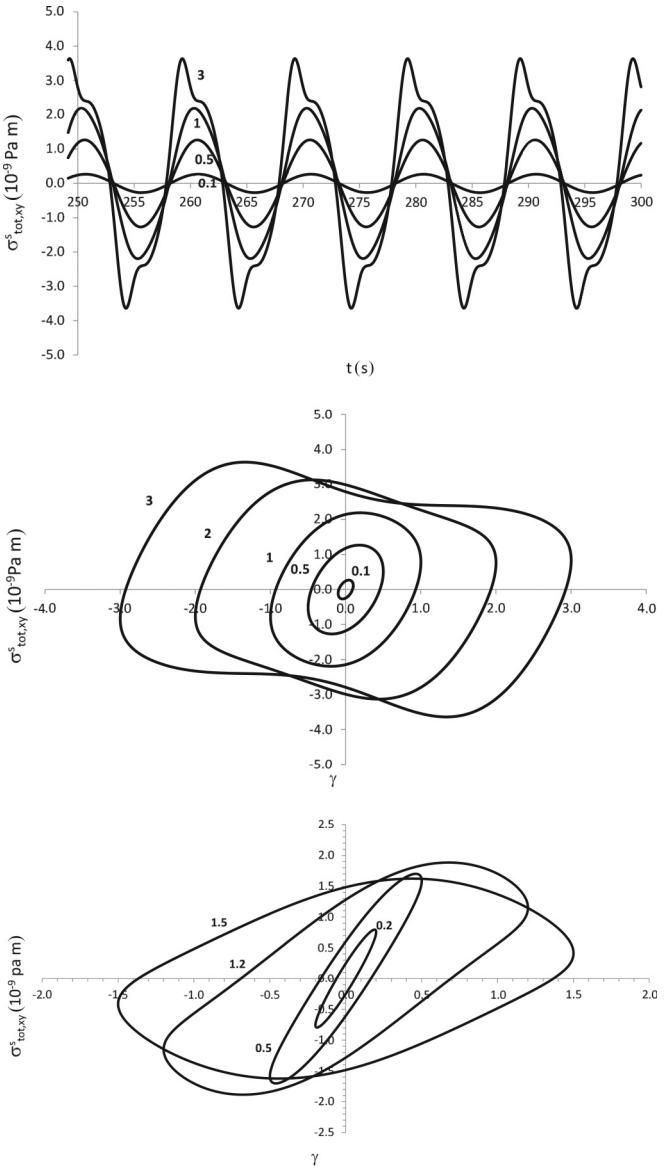

FIG. 7. (a) Shear stress for an oscillatory in-plane shear deformation as a function of time ($\omega = 0.1$, $\tau = 1.0$); (b) Lissajous plots for $\omega\tau = 0.1$; (c) Lissajous plots for $\omega\tau = 1.0$. Labels indicate the strain amplitude γ_0. Other parameters: $T^s = 290$ K, $\rho^s = 1 \times 10^{-6}$ kg/m^2, $\omega_P^s = 0.01$, $m = 1 \times 10^{-20}$ kg, $\varepsilon_s = 1 \times 10^{-9}$ Pa m s^{-1}.

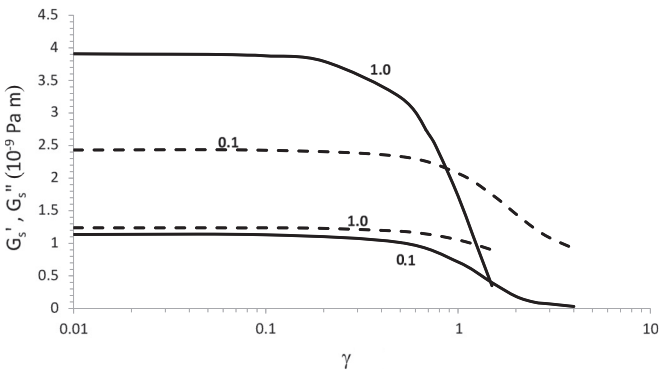

FIG. 8. G_s' (solid curves) and G_s'' (dashed curves) vs strain γ for two values of $\omega\tau$, equal to 0.1 and 1 (see labels).

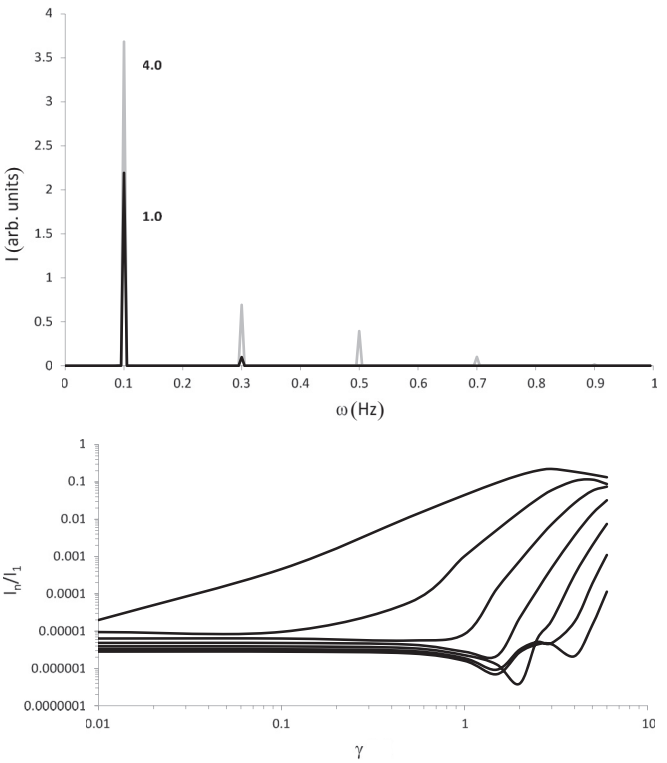

FIG. 9. (a) FT spectrum of the surface stress response to an oscillatory deformation with applied frequency ω, equal to 0.1; τ is equal to 1.0; for the grey curve $\gamma_0 = 4.0$, and for the black curve $\gamma_0 = 1.0$. (b) Normalized intensities I_n/I_1 as a function of strain amplitude for (from top to bottom) $n = 3$, 5, 7, 9, 11, 13, and 15.

1.0. These moduli were calculated using $G_s' = (\sigma_0/\gamma_0)\cos\delta$ and $G_s'' = (\sigma_0/\gamma_0)\sin\delta$. For $\omega\tau = 1.0$ we see that in the linear response regime $G_s' > G_s''$, which implies $\tan\delta < 1$, and the interface displays solid elastic behavior. At a strain amplitude of about 0.2 both the surface storage and loss modulus start to decrease significantly with increasing amplitudes, and at a strain slightly above 1.0 a crossover from elastic to more viscous behavior occurs. At low values for $\omega\tau$ we see that $G_s' < G_s''$ and $\tan\delta > 1$ for the entire range of amplitudes.

To study the nonlinear response of the interface more accurately, we determined the intensities of the higher harmonics in the stress response. Figure 9(a) shows a typical spectrum of the stress, for $\omega\tau = 0.1$, and two values of the strain amplitude (1.0 and 4.0 respectively). The spectrum shows only odd harmonics (odd multiples of the applied frequency), and this indicates that the response of the microstructure is identical for clockwise and counterclockwise motion. In the spectrum of $\gamma_0 = 4.0$ the highest harmonic we could detect was I_{15}. In Fig. 9(b) we have plotted the normalized intensity of the harmonics, I_n/I_1 ($n = 3,5,7,9,11,13,15$), as a function of the applied strain amplitude. We see that even at strains as low as 0.01 there is already a small contribution of the third harmonic to the stress response, showing that systems such as the one we are studying here display nonlinear behavior at very low strains. At a strain as low as about 0.1, the fifth harmonic starts to contribute to the stress response, and at strains slightly above 1, we can detect contributions from the 7th through the 15th harmonic. An analysis like the one presented in Fig. 9(b) illustrates

the usefulness of FT rheology for studying the rheology of interfaces with a complex microstructure.

V. OSCILLATORY DILATATIONAL FLOW

We will now examine the predictions of our model for an interface perturbed by an oscillatory dilatational flow. We will choose a flow pattern similar to that encountered in a Langmuir trough, so we assume a strain in the x direction given by $\gamma_{xx}(t) = \gamma_0 \sin(2\pi\omega t)$. The components of the velocity gradient tensor are therefore given by

$$(\nabla_s \mathbf{v}^s)_{xx}(t) = \dot{\gamma}_{xx} = 2\pi\omega\gamma_0 \cos(2\pi\omega t) \tag{22}$$

and $(\nabla_s \mathbf{v}^s)_{xy} = (\nabla_s \mathbf{v}^s)_{yx} = (\nabla_s \mathbf{v}^s)_{yy} = 0$. For this type of flow the xx component of the surface extra stress tensor is given by [using Eq. (9)]

$$\sigma^s_{\mathrm{tot},xx} = (\varepsilon_d + \varepsilon_s)\,\dot{\gamma}_{xx} + \left(\frac{k_B T^s \rho^s \omega_P^s}{m}\right)\left(C^s_{xx} - 1\right). \tag{23}$$

Using (8) we obtain for the xx and xy components of $\mathbf{C}^s$ (setting $\beta = 0$)

$$\frac{\partial C^s_{xx}}{\partial t} = 2\dot{\gamma}_{xx}(t) C^s_{xx} - \frac{1}{\tau}\left(C^s_{xx} - 1\right), \tag{24}$$

$$\frac{\partial C^s_{xy}}{\partial t} = \dot{\gamma}_{xx}(t) C^s_{xy} - \frac{1}{\tau} C^s_{xy}. \tag{25}$$

With initial condition $\mathbf{C}^s(0) = \mathbf{P}$, the solution of (25) is of course $C^s_{xy}(t) = 0$, and we only have to solve (24) numerically. This equation was solved with the same scheme we used for the oscillatory shear calculations discussed in the previous section. Figure 10 shows Lissajous plots for oscillations with an applied frequency of 0.1 Hz, and a relaxation time τ equal to 1.0 s. Strain amplitudes γ_0 range 0.1–0.5. Note that these strains are much smaller than the ones we applied in the shear simulations. The strain in this type of flow is defined as $\gamma_{xx} = \Delta A/A_0$, where ΔA denotes the change in surface area, and A_0 is the initial surface area. In compression at a strain close to 1.0 we would approach the 2D close packing limit of the particles (since we have assumed the particles are adsorbed irreversibly at the interface). At such high strains interfaces tend to show buckling, and parameters like the bending rigidity

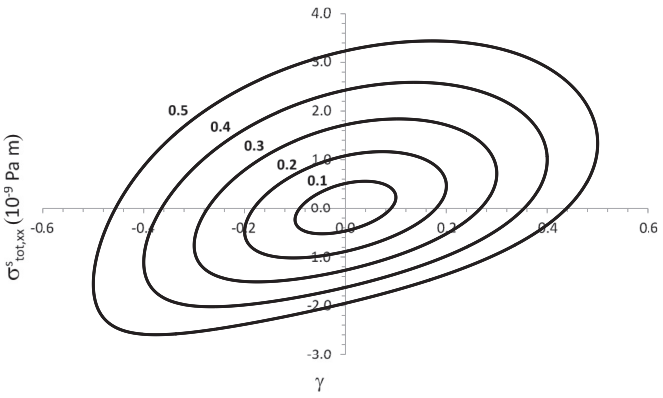

FIG. 10. Lissajous plot for an oscillatory dilatational deformation with ω equal to 0.1 Hz, and τ equal to 1 s; labels indicate the strain amplitude γ_0. Other parameters: $T^s = 290$ K, $\rho^s = 1 \times 10^{-6}$ kg/m^2, $\omega_P^s = 0.01$, $m = 1 \times 10^{-20}$ kg, $\varepsilon_s = \varepsilon_d = 1 \times 10^{-9}$ Pa m s^{-1}.

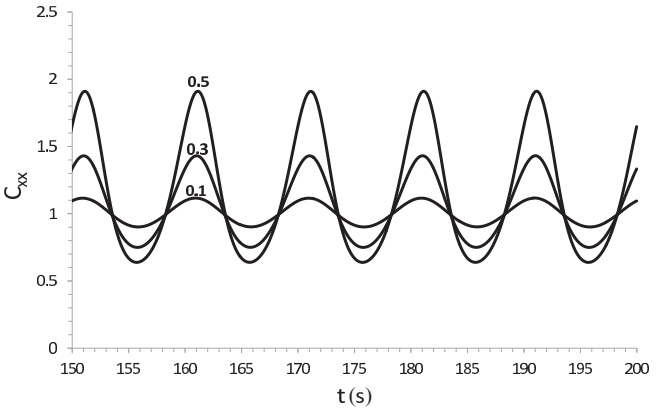

FIG. 11. C^s_{xx} as a function of time for a frequency ω equal to 0.1 Hz, and τ equal to 1 s; labels indicate the strain amplitude γ_0. Other parameters: $T^s = 290$ K, $\rho^s = 1 \times 10^{-6}$ kg/m^2, $\omega_P^s = 0.01$, $m = 1 \times 10^{-20}$ kg, $\varepsilon_s = \varepsilon_d = 1 \times 10^{-9}$ Pa m s^{-1}.

of the interface become important. This is not only true for particle stabilized interfaces but also for many other types of interfaces with a complex microstructure [31–37]. Since effects like these are not accounted for in our model we have limited the maximum strain in our simulations to 0.5.

When looking at Fig. 10 not only do we see the onset of nonlinear behavior at very low strains, but we also see an asymmetry develop in the stress cycle: the maximum stress in the extension part of the cycle is significantly higher than the absolute value of the maximum stress in the compression part of the cycle.

Of course, since we have assumed that the particles are irreversibly adsorbed at the interface, their concentration changes as we deform the interface: the concentration increases in the compression part of the cycle, and decreases in the extension part of the cycle. This however would amplify the stress in the compression phase, whereas we see in Fig. 10 that the extension phase is amplified with respect to the compression part of the cycle.

In Fig. 11 we can clearly see that the asymmetry in the cycle is caused by a difference in the orientation of the particles in the extension and compression parts of the cycle. At a strain of 0.5 the maximum in C_{xx} in the extension part of the cycle is about 1.8, which means the particles are predominantly aligned in the x direction. In the compression part of the cycle the minimum value for C_{xx} is about 0.6, and since $C_{xx} + C_{yy} = 2$, we find $C_{yy} \approx 1.4 > C_{xx}$. So, in this part of the cycle the particles are aligned predominantly in the y direction. When particles are aligned in the x direction, they are aligned parallel to the velocity gradient direction, whereas when they are aligned in the y direction, they are aligned perpendicular to the velocity gradient direction. When particles are aligned perpendicular to the velocity gradient direction their contribution to the stress is much smaller than when they are oriented parallel to the velocity gradient direction. This example clearly illustrates the benefits of analyzing the nonlinear behavior of complex interfaces using structural parameters.

In Fig. 12 we see that the asymmetry in the stress cycle leads to the emergence of even harmonics in the frequency spectrum of the surface stress. These even harmonics have been detected

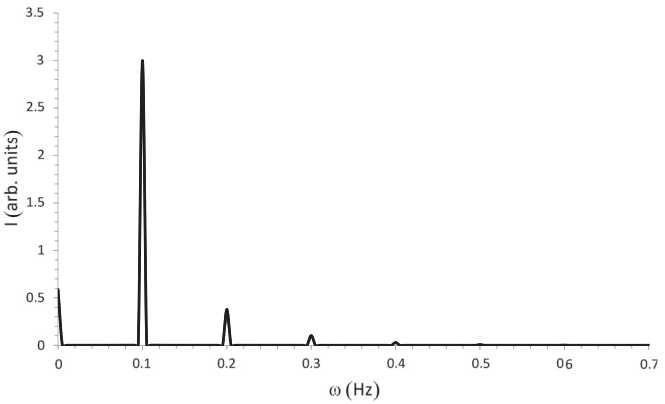

FIG. 12. FT spectrum for an oscillatory dilatational deformation with applied frequency ω equal to 0.1 Hz, and strain amplitude γ_0 equal to 0.5.

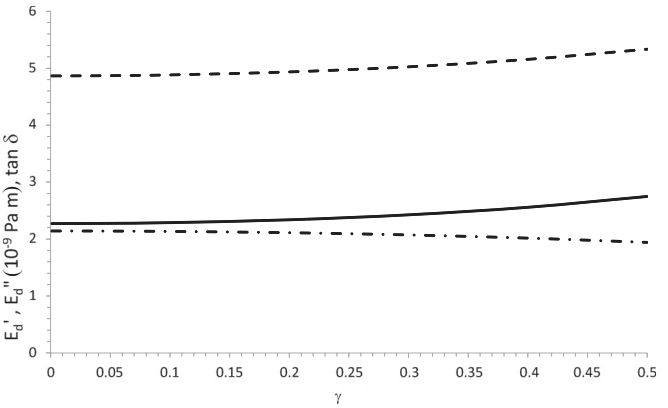

FIG. 14. Oscillatory dilatational strain sweep at a frequency ω equal to 0.1 Hz, and τ equal to 1 s. Dashed curve: E_d''; solid curve: E_d'; dash-dotted curve: $\tan\delta$.

experimentally in oscillatory dilatational measurements on polymer stabilized interfaces [16,17]. The explanation for the occurrence of even harmonics in polymer stabilized interfaces is similar to what we have observed for anisotropic colloidal particles: upon compression of the interface polymer segments are predominantly oriented in the y direction, whereas upon extension of the interface polymer segments are predominantly oriented in the x direction.

Figure 13 shows the normalized intensity I_n/I_1 of even and odd harmonics, as a function of the applied strain amplitude. We see that at strains as low as 0.001 there is already a detectable second harmonic in the stress response. At a strain of 0.01 the third harmonic starts to contribute, and at strains around 0.1 we have a highly nonlinear response with contributions from the 4th through the 16th harmonic.

In Fig. 14 we have plotted the dilatational storage modulus $E_d' = (\sigma_0/\gamma_0)\cos\delta$, the dilatational loss modulus $E_d'' = (\sigma_0/\gamma_0)\sin\delta$, and the dilatational loss tangent $\tan\delta = E_d''/E_d'$. In contrast to the surface shear experiments we see a mild shear thickening behavior as a function of increasing strain amplitude. The difference between the response in dilatational flow and surface shear flow, where we saw shear thinning behavior, can again be explained in terms of differences in particle orientation, induced by these flow types. In oscillatory shear deformations the particles were aligned perpendicular to the velocity gradient direction, leading to a decrease of the contribution of the particles to the surface shear stress, and hence to shear thinning behavior. In dilatational deformations the particles are oriented by the flow in a direction parallel to the velocity gradient (at least in the extension part of the cycle, which clearly dominates the stress response), and this leads to shear thickening.

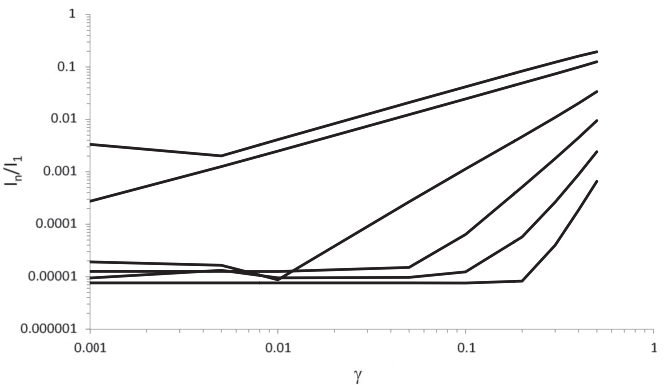

FIG. 13. Normalized intensities I_n/I_1 as a function of applied strain amplitude, at a frequency ω equal to 0.1 Hz.

VI. CONCLUSIONS

In this paper we have presented a GENERIC model for the rheological behavior of an interface stabilized by a dilute 2D dispersion of anisotropic colloidal particles. The dependence of the surface stress on the microstructure of the interface was incorporated through a single tensorial structural variable, describing the average of the orientation of the particles. We have examined the predictions of this model in steady in-plane shear, oscillatory in-plane shear, and oscillatory dilatational flow. In both steady and oscillatory shear flow the model predicts shear thinning behavior, which has also been observed experimentally for this type of interface. This behavior is the result of an increasing orientation of the particles perpendicular to the velocity gradient direction, for increasing shear rate (or strain amplitude). FT analysis showed us that this type of interface starts to display nonlinear behavior at strains as low as 0.01. In shear the frequency spectrum displays only odd multiples of the applied frequency.

For dilatational deformations we observed a mild strain thickening behavior for increasing strain. The FT spectrum of the stress response displays even as well as odd harmonics. The even harmonics are the result of an asymmetry in the stress response between the compression and extension part of the deformation cycle. Particles tend to orient parallel to the velocity gradient direction in the extension part of the cycle, and perpendicular to the velocity gradient direction in the compression part of the cycle. As a result of this difference in orientation the stresses in the extension cycle are higher than the stresses generated in compression.

Our analysis shows the benefits of analyzing the highly nonlinear rheological response of interfaces with a complex microstructure using structural models. In bulk rheology this

type of modeling has been applied successfully to a wide range of systems, such as polymer melts and solutions, or liquid crystalline phases [13,14]. Structural models have found only limited application in the analysis of nonlinear rheological data for complex interfaces [15]. Rey [38–40] used structural variables to model the surface rheology of nematic polymer-viscous fluid interfaces, and Oh *et al*. [41] used a structural model to describe the interfacial behavior in single wall carbon nanotubes. We envision that structural models like the one we have presented here, combined with advanced experimental techniques such as FT rheology and optical methods for structure evaluation (surface rheo-optics), will allow us to make significant progress in the study of the dynamics of complex interfaces.

[1] S. Pickering, J. Chem. Soc. **91**, 2001 (1907).
[2] K. P. Velikov, F. Durst, and O. D. Velev, Langmuir **14**, 1148 (1998).
[3] B. P. Binks, Curr. Opin. Colloid Interface Sci. **7**, 21 (2002).
[4] S. Reynaert, P. Moldenaers, and J. Vermant, Phys. Chem. Chem. Phys. **9**, 6463 (2007).
[5] K. Masschaele, J. Fransaer, and J. Vermant, J. Rheol. **53**, 1437 (2009).
[6] F. Ravera, E. Santini, G. Loglio, M. Ferrari, and L. Liggieri, J. Phys. Chem. B **110**, 19543 (2006).
[7] F. Ravera, M. Ferrari, L. Liggieri, G. Loglio, E. Santini, and A. Zanobini, Colloids Surf. A **323**, 99 (2008).
[8] H. Wang, Y. Gong, W. Lu, and B. Chen, Appl. Surf. Sci. **254**, 3380 (2008).
[9] X. Dong, J. Xu, C. Cao, D. Sun, and X. Jiang, Colloids Interfaces A **353**, 181 (2010).
[10] B. Madivala, J. Fransaer, and J. Vermant, Langmuir **25**, 2718 (2009).
[11] P. F. Noble, O. J. Cayre, R. G. Alargova, O. D. Velev, and V. Paunov, J. Am. Chem. Soc. **126**, 8092 (2004).
[12] M. G. Basavaraj, G. G. Fuller, J. Fransaer, and J. Vermant, Langmuir **22**, 6605 (2006).
[13] R. G. Larson, *The Structure and Rheology of Complex Fluids* (Oxford University Press, Oxford, 1999).
[14] H. C. Öttinger, *Beyond Equilibrium Thermodynamics* (Wiley-Intersience, Hoboken, 2005).
[15] L. M. C. Sagis, Rev. Mod. Phys. **83**, 1367 (2011).
[16] H. M. Hilles, F. Monroy, L. J. Bonales, F. Ortega, and R. G. Rubio, Adv. Colloid Interface Sci. **122**, 67 (2006).
[17] H. M. Hilles, A. Maestro, F. Monroy, F. Ortega, R. G. Rubio, and M. G. Velarde, J. Chem. Phys. **126**, 124904 (2006).
[18] L. M. C. Sagis, Soft Matter **17**, 7727 (2011).
[19] J. C. Slattery, L. M. C. Sagis, and E. S. Oh, *Interfacial Transport Phenomena*, 2nd ed. (Springer, New York, 2007).
[20] G. C. Sarti and G. Marrucci, Chem. Eng. Sci. **28**, 1053 (1973).
[21] J. Boussinesq, C. R. Seances Acad. Sci., Ser. **156**, 983 (1913).
[22] J. Boussinesq, C. R. Seances Acad. Sci., Ser. **156**, 1035 (1913).
[23] J. Boussinesq, C. R. Seances Acad. Sci., Ser. **156**, 1124 (1913).
[24] L. M. C. Sagis and H. C. Öttinger, Phys. Rev. E **88**, 022149 (2013).
[25] P. Erni, P. Fischer, E. J. Windhab, V. Kusnezov, H. Stettin, and L. Läuger, Rev. Sci. Instrum. **74**, 4916 (2003).
[26] P. Erni, P. Fischer, P. Heyer, E. J. Windhab, V. Kusnezov, and L. Läuger, Prog. Colloid Polym. Sci. **129**, 16 (2004).
[27] D. A. Edwards, H. Brenner, and D. T. Wasan, *Interfacial Transport Phenomena and Rheology* (Butterworth-Henemann, Boston, 1991).
[28] M. Wilhelm, D. Maring, and H. W. Spiess, Rheol. Acta **37**, 399 (1998).
[29] M. Wilhelm, P. Reinheimer, and M. Ortseifer, Rheol. Acta **38**, 349 (1999).
[30] L. M. C. Sagis, M. Ramaekers, and E. van der Linden, Phys. Rev. E **63**, 051504 (2001).
[31] J. B. A. F. Smeulders, C. Blom, and J. Mellema, Phys. Rev. A **42**, 3483 (1990).
[32] J. B. A. F. Smeulders, J. Mellema, and C. Blom, Phys. Rev. A **46**, 7708 (1992).
[33] K. H. de Haas, G. J. Ruiter, and J. Mellema, Phys. Rev. E **52**, 1891 (1995).
[34] E. Scholten, L. M. C. Sagis, and E. van der Linden, J. Phys. Chem. B **108**, 12164 (2004).
[35] E. Scholten, L. M. C. Sagis, and E. van der Linden, Macromolecules **38**, 3515 (2005).
[36] E. Scholten, L. M. C. Sagis, and E. van der Linden, J. Phys. Chem. B **110**, 3250 (2006).
[37] L. M. C. Sagis, J. Controlled Release **131**, 5 (2008).
[38] A. D. Rey, Rheol. Acta **39**, 13 (2000).
[39] A. D. Rey, Macromol. Theory Simul. **9**, 156 (2000).
[40] A. D. Rey, Eur. Phys. J. E **2**, 169 (2000).
[41] E. S. Oh, D. C. Lagoudas, and J. C. Slattery, Philos. Mag. **85**, 2249 (2005).